The Magic of Carrier Fringes in Moiré Interferometry

by Y. Guo, D. Post and R. Czarnek

ABSTRACT—Practical applications in which carrier fringes are used with moiré interferometry for strain measurements are presented. Examples illustrate how moiré carrier fringes are applied to obtain the desired data in complex laminated composite specimens. In many cases, carrier fringes permit extraction of much more detailed information, with procedures that are easier and more accurate than those using load-induced fringes alone. The fringe vector for carrier fringes is introduced and its application to the interpretation of fringe patterns is explained. In moiré interferometry, the carrier fringes are produced easily by adjustments of optical elements that control the virtual reference grating.

Introduction

In geometric moiré, the carrier fringes have been called *mismatch fringes.*[1,2] They are introduced by changing the frequency or the direction of the reference grating. In the case of moiré interferometry, a very large number of carrier (or mismatch) fringes is sometimes introduced—even many times the number of load-induced fringes. In such cases, a high-frequency pattern of uniformly spaced carrier fringes is modulated by the load-induced changes of fringe orders. The analogy to carrier frequencies in communications technology is strong, and similar terminology is adopted. As used here, the terms *carrier fringes* and *carrier patterns* represent any carrier fringe frequency: high or low, positive or negative. These carrier fringes can increase or decrease the frequency of load-induced fringes.

The term *mismatch* does not apply consistently to moiré interferometry. The word implies a difference in frequency or orientation of specimen reference gratings. However, moiré interferometry can operate when there is no reference grating at all*—neither a real reference grating nor a virtual reference grating—but nevertheless carrier fringes can be produced in such a case. The term *carrier* is meaningful even when *mismatch* is not, so *carrier fringes* will be the terminology favored here.

The carrier pattern is an important ingredient in moiré interferometry. Together with other special properties, it makes moiré interferometry a unique and powerful technique for displacement and strain measurements. Carrier patterns can be used for various purposes, including the following: (1) to increase the accuracy of extracting data from a fringe pattern; (2) to distinguish the signs of the displacements by introducing a carrier pattern of known sign; (3) to determine fringe gradients when they are not adequately represented in the load-induced fringe patterns; (4) to cancel the initial or no-load fringe pattern; and (5) to measure in-plane and out-of-plane displacements simultaneously.

All the applications mentioned above have their own magic qualities. In this paper, the third issue is illustrated by several examples. The details of other applications can be found in Refs. 1-5.

Moiré Interferometry

Basic Principle

In moiré interferometry,[3] a diffraction grating is replicated on the specimen and it deforms together with the loaded specimen. A virtual reference grating created by interference of two coherent beams, B_1 and B_2 (depicted in Fig. 1), is superimposed on the specimen grating.

Y. Guo is Graduate Project Assistant, D. Post (SEM Fellow) is Professor, and R. Czarnek (SEM Member) is Assistant Professor, Engineering Science and Mechanics Department, Virginia Polytechnic Institute and State University, Blacksburg, VA 24061.

Original manuscript submitted: February 1988. Final manuscript received: September 16, 1988.

**Consider Beam B_1 and B_2 in Fig. 1 when their polarizations are in the horizontal plane, i.e., perpendicular to the y axis. Then, when α = 45 deg, the two beams are orthogonally polarized, so they cannot interfere to produce a virtual reference grating. Nevertheless, the diffracted beams that reach the camera have parallel polarizations and they interfere to create the moiré pattern. A rigorous explanation of moiré interferometry (Ref. 3, pp. 335-338) does not involve a reference grating.*

If polarizations of B_1 and B_2 are parallel to y, a virtual reference grating is produced and a casual explanation utilizing the virtual reference grating is given in the next section.

The specimen and reference gratings interact to form a fringe pattern N_x, which is a contour map of in-plane specimen displacements U. This pattern is photographed with a camera focused on the specimen surface. Beams B_3 and B_4 (not shown), lying in the vertical plane, interact with the specimen grating to form the N_y pattern and the V displacement field. In Fig. 1, f is the frequency of the virtual reference grating and N is the fringe order at each point in the moiré pattern. In this work, f = 2400 ℓ/mm, or 60,960 ℓ/in.

Moiré Carrier Patterns

In moiré interferometry, the direction and the frequency of the reference grating is changed by adjusting the incident beam B_1 or B_2 (Fig. 1). Experimentally, this is usually done by a thumbscrew adjustment of one optical element, e.g., a mirror that directs light into B_1. A carrier pattern of extension, composed of fringes parallel to the lines of the specimen grating, is obtained by a small change of the magnitude of angle 2α. A carrier pattern of rotation, composed of fringes essentially perpendicular to the lines of the specimen grating, is obtained by a small out-of-plane inclination of B_1 or B_2, or by a small rigid-body rotation of the specimen grating.

Fringes and Fringe Vectors

There are two ways to obtain fringes. One is to deform the specimen grating by external loads or other means, and the other one is to change the reference grating. (Rotation of the specimen relative to the reference grating is equivalent to changing the reference grating.) The first one introduces load-induced fringes and the second one introduces carrier fringes.

The fringe gradient has vector properties as illustrated in Fig. 2. At any point, a fringe vector F is defined such that it is perpendicular to the tangent to the fringe at that point and has a direction toward the direction of increasing fringe orders. Its length, or magnitude, is proportional to the gradient of the fringes along the defined direction. All the rules of vector calculation can be applied to the fringe vector. A fringe vector can be decomposed into two orthogonal components F_x and F_y which are related by the equation

$$F_y = F_x \tan \phi \tag{1}$$

where F_x and F_y represent the fringe gradients $\partial N/\partial x$ and $\partial N/\partial y$ respectively, and tan ϕ is the slope of the fringe vector (or the reciprocal of the slope of the fringe).

When a carrier pattern is introduced, the resultant fringe vector is equal to the vector sum of the load-induced fringe vector and the fringe vector of the carrier pattern. At any point of the fringe pattern

$$F_x = F_{lx} + F_{cx} \qquad F_y = F_{ly} + F_{cy} \tag{2}$$

where subscript l represents the load-induced fringes and subscript c represents the carrier fringes. Thus, eq (1) can be written as

$$F_{ly} + F_{cy} = (F_{lx} + F_{cx}) \tan \phi \tag{3}$$

In terms of the fringe vector and its components, the displacement derivatives can be calculated by the following equations. For the U (x-direction) displacement field,

$$\frac{\partial U}{\partial x} = \frac{1}{f} F_{lx} \qquad \frac{\partial U}{\partial y} = \frac{1}{f} F_{ly} \tag{4}$$

and for the V (y-direction) displacement field,

$$\frac{\partial V}{\partial y} = \frac{1}{f} F_{ly} \qquad \frac{\partial V}{\partial x} = \frac{1}{f} F_{lx} \tag{5}$$

The strains can be determined by the well-known small deformation equations

$$\epsilon_x = \frac{\partial U}{\partial x} \qquad \epsilon_y = \frac{\partial V}{\partial y} \tag{6}$$

$$\gamma_{xy} = \frac{\partial U}{\partial y} + \frac{\partial V}{\partial x} \tag{7}$$

It is evident that the carrier fringes are not required, in principle, to determine strains. Carrier fringes can be used, however, to transform the pattern to one from which the load-induced gradients can be extracted with enhanced precision and ease. These virtues are illustrated by the applications that follow.

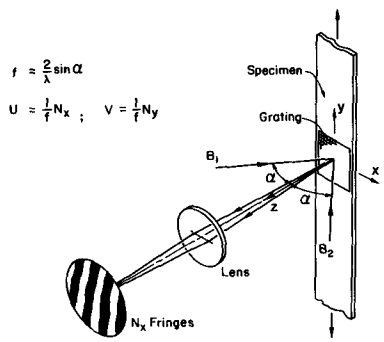

Fig. 1—Moiré interferometry and relevant equations

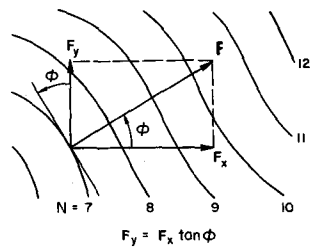

Fig. 2—Fringe azimuth and fringe vectors

Carrier Fringes of Rotation

Carrier fringes of rotation are oriented perpendicular to the bisector of the initial specimen grating lines and the reference grating lines. Consequently, the carrier fringe vector has two components which are functions of θ:

$$F_c = \theta f \qquad F_e = -\frac{\theta^2 f}{2} \tag{8}$$

where θ is the small angle between the initial specimen grating lines and the reference grating lines; F_c is the desired component of the carrier fringe vector of rotation and lies parallel to the specimen grating lines; and F_e is the extraneous component of the carrier fringe vector and lies perpendicular to F_c. For a fixed coordinate system aligned with the initial orientation of the specimen

grating lines, the extraneous component F_e is always negative. It is an apparent uniform compressive strain on the specimen surface. In practice, angle θ is usually very small and the extraneous component is usually negligible. For example, if F_c is 10 fringes/mm and the frequency (f) of the reference grating is 2400 ℓ/mm, we find that θ is 0.004 radians, and F_e is 0.02 fringes/mm. The apparent extraneous strain ϵ_e is -9 μm/m. Thus, the effects are very small. When a very strong carrier pattern of rotation is used in some special cases, however, the extraneous effects might not be negligible. In such cases, corrections can be applied.

The carrier pattern of rotation can be produced in two ways: (1) by rigid-body rotation of either the specimen grating or the reference grating relative to the other; or (2) by adjustment of beam B_1 (and/or B_2) illustrated in Fig. 1. Equations (8) apply directly to case (1). For case (2), one must consider the great variety of optical systems that can be used to produce beams B_1 and B_2.[3,6] No common analysis can be given for the carrier fringes in terms of the adjustments of the mirrors or optical elements. Instead, means to maintain F_e within acceptable limits must be considered on an individual basis.

Applications of Carrier Fringes

Specimens

In the studies illustrated here, the specimens were all made from laminated fiber-reinforced composite materials. Interlaminar deformations were examined. For experimental analyses of the behavior of these complex structural bodies, moiré interferometry and its carrier patterns have provided an excellent and unique approach.

Carrier Fringes Parallel to the Initial Fringes

Figure 3 shows a rail-shear test for determination of interlaminar deformations of a graphite-epoxy specimen with a $[90/90/0]_n$ stacking sequence. Figure 3(b) is the fringe pattern of the load-induced V displacement field in the central part of the specimen. The cross derivative $\frac{\partial V}{\partial x}$ is very high, corresponding to a large magnitude of fringe vector F_{lx}, and the fringes are nearly vertical. If the strain ϵ_y (corresponding to the gradient F_{ly}) is desired, its determination from this pattern would be difficult. By introducing carrier fringes of rotation, which are nearly parallel to the load-induced fringes, the fringe pattern is simplified while the fringe vector F_{ly} remains essentially unchanged. This is illustrated in Fig. 3(c), where the carrier fringes minimize the resultant F_x, i.e., the gradient of carrier fringes F_{cx} nearly cancels F_{lx}. Now, the gradient F_{ly} at any point can be determined easily.

Carrier Fringes Perpendicular to the Initial Fringes

If the shear strain component $\frac{\partial V}{\partial x}$ is required from Fig. 3(b), the fringe vector F_{lx} has to be obtained. Because the specimen is fabricated with successive plies of 90-deg and 0-deg fiber orientations, the shear strains vary from ply to ply. In certain plies, the deformations are represented by only one fringe. It is impossible to measure the gradient by only one fringe (unless a sophisticated grey-level technique with very high spatial resolution is applied). By introducing a carrier pattern of extension F_{cy}, the fringe pattern is transformed to that of Fig. 3(d). The fringe vector F_{lx} can be calculated by eq (3) as $F_{lx} = F_y/\tan\phi$, where $F_y = F_{ly} + F_{cy}$. The fringe gradient F_y is easily

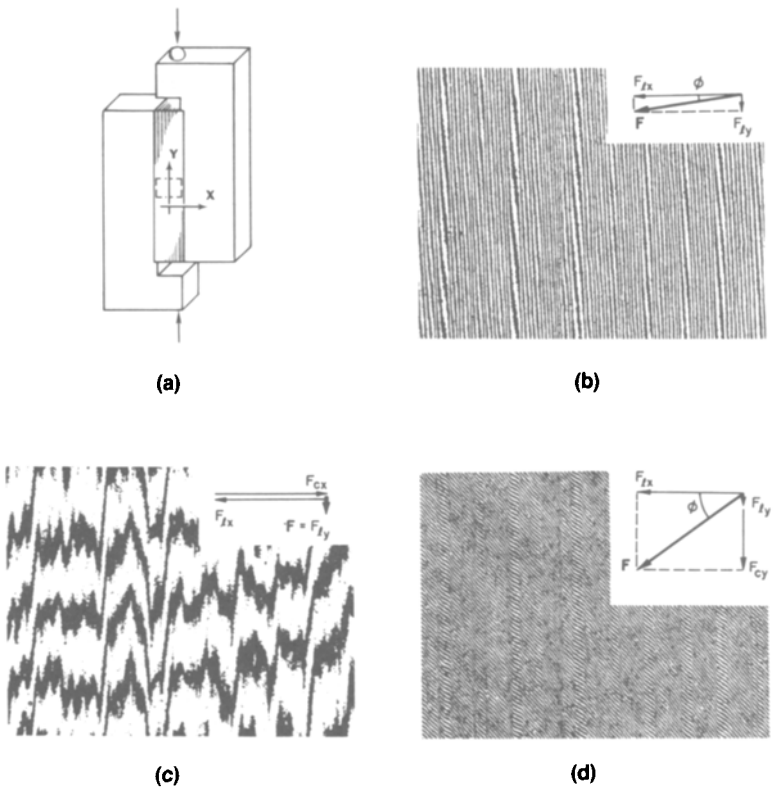

Fig. 3—Rail-shear test for interlaminar deformations of $[90/90/0]_n$ graphite-epoxy composite specimen. Inserts on patterns show the corresponding fringe vectors. (a) Specimen and loading fixture. (b) Load-induced fringe pattern of the V field for portion of specimen in dashed box. (c) Load-induced fringes with carrier fringes of rotation. (d) Load-induced fringes with carrier fringes of extension

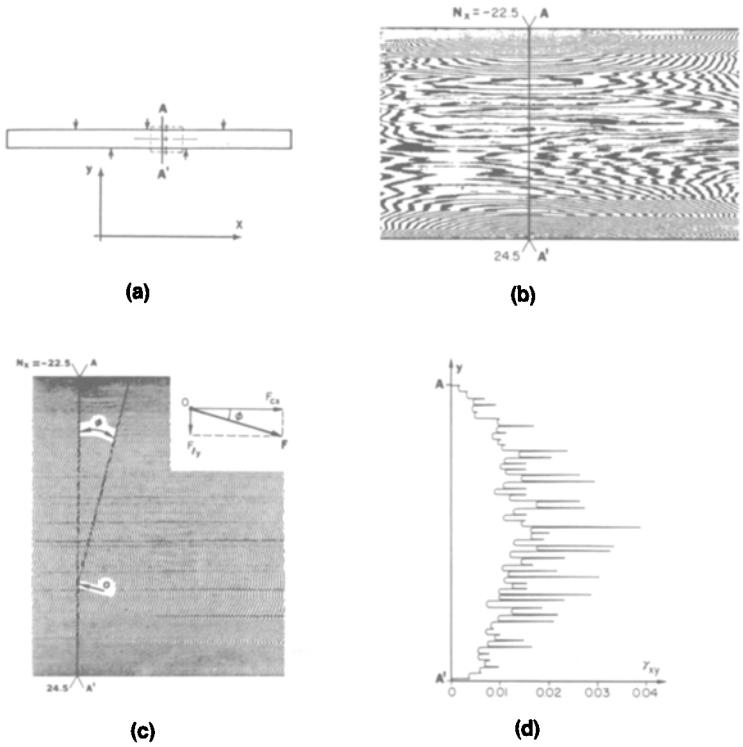

Fig. 4—Five-point bending test of $[+45/0/-45/90]_{6s}$ graphite-PEEK composite beam. (a) Specimen and loading. (b) Load-induced fringe pattern of the U field for portion of specimen in dashed box. (c) Load-induced fringes with carrier fringes of extension. (d) Shear strain distribution along line A-A′

determined in any region from Fig. 3(d) by measuring the vertical (y) distance between fringes. At any point in the pattern, ϕ is determined by the angle of the fringe normal at that point. As a practical matter, the method is implemented best when ϕ is approximately 45 deg. Since the carrier pattern does not affect the fringe vector in the x direction, F_{lx} still represents the required gradients $\frac{\partial V}{\partial x}$. The gradients are revealed at every point in the field because the fringe angle (and F_y) can be determined at any point. Gradients $\frac{\partial V}{\partial x}$ that could not be recognized from Fig. 3(b) can be calculated with high fidelity from Fig. 3(d).

Detailed normal and shear strain distributions are presented in Ref. 7 for this specimen. Dramatic variations of shear strains were found, including relatively large shear strains in resin-rich zones between plies.

Figure 4 is another example of the use of a perpendicular carrier pattern. The specimen is a 48-ply quasi-isotropic beam of graphite-PEEK in a five-point bending test.[8] Figure 4(b) depicts the load-induced U displacement field. The pattern is complicated and it is difficult to assign fringe orders in the central region with certainty. In addition, there are insufficient fringes in the central region to determine the strain in each ply. However, carrier fringes of extension F_{cx} transform the pattern to that of Fig. 4(c). Now the fringes can be traced without ambiguity. The gradient F_{ly} in the different plies, along AA′, can be determined from the fringe angles by eq (3), where F_{lx} and F_{cy} equal zero; it reduces to $F_{ly} = F_{cx} \tan \phi$ as shown in the vector diagram [Fig. 4(c)] for point 0. The shear strain distribution along line AA′ was calculated by eq (7) and plotted in Fig. 4(d), using data from this pattern and the corresponding V field. The different strain levels in successive plies are caused by their different stiffnesses in shear. The high peaks occur at the resin-rich zones between plies, where high shear compliance leads to localized high shear strains.

Carrier Fringes in Both Directions

Figure 5 illustrates an interlaminar compression test of a thick composite. The material was graphite-epoxy with a $[90/90/0]_n$ stacking sequence, i.e., two plies with fibers in the z direction followed by one ply with fibers in the x direction, repeated many times. The specimen was 15-mm tall with 13 × 13 mm cross section.

The V displacement field is shown in Fig. 5(a) for the portion in the dashed box. The strains could be determined easily in the 90-deg plies by $\epsilon_y = F_{ly}/f$. In the 0-deg plies, however, the fringes are too few to determine their gradient. The pattern was transformed to that of Fig. 5(b) by adding carrier patterns of both extension and rotation. First, a carrier pattern of extension was applied; it was equal in magnitude and opposite in sign to the fringe gradient in 90-deg plies, such that the fringe gradient in 90-deg plies was cancelled. Then a carrier pattern of rotation was applied to produce Fig. 5(b). Near point A, the fringes in 90-deg plies are vertical, which indicates that the y component of the resulting fringe vector is zero. In 0-deg plies the fringes have a direction ϕ_1, and in resin-rich zones between plies they have a direction ϕ_2. The corresponding strains ϵ_y are calculated by using eqs (3), (5) and (6), from which

$$\epsilon_y = \frac{1}{f} F_{cx} \tan \phi + \epsilon_{90}$$
$$\epsilon_{90} = -\frac{1}{f} F_{cy} \tag{9}$$

where ϵ_{90} is the normal strain in the 90-deg plies, i.e., the strain that was subtracted off by introducing $F_{cy} = -F_{ly}$. Equation (9) is an implementation of eq (3) where both F_{cx} and F_{cy} are nonzero.

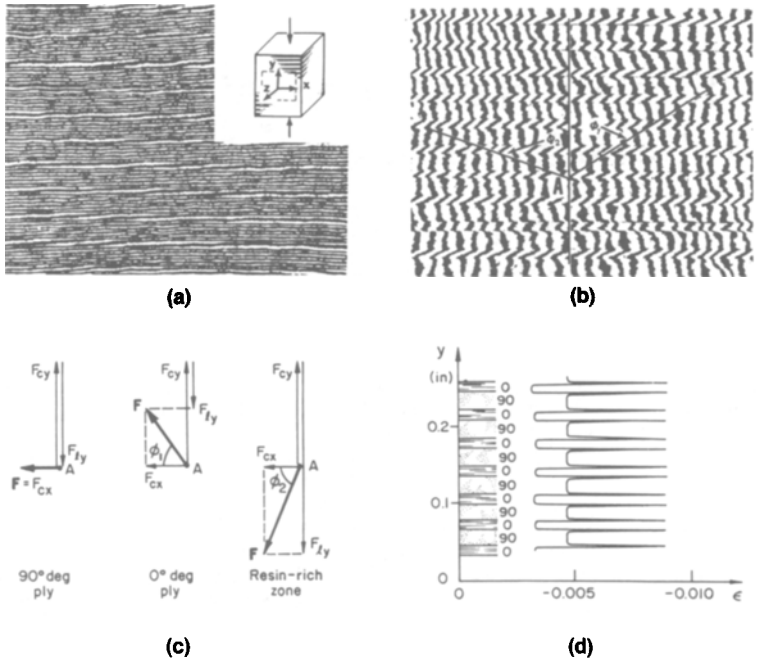

Fig. 5—Interlaminar compression test of $[90/90/0]_n$ graphite-epoxy composite specimen. (a) Load-induced fringe pattern of the V field for portion of specimen in dashed box. (b) Load-induced fringes with carrier fringes of extension and rotation. Near point A, fringe angles are zero and ϕ_1 in the 90-deg and 0-deg plies, respectively, and ϕ_2 in the resin-rich zone between plies. (c) Fringe vector diagrams. (d) Compressive strain distribution along a vertical line. Note this is schematic since material properties and strain vary along each ply and between corresponding plies

The pattern of Fig. 5(b) is interpreted by fringe vectors in Fig. 5(c). In 90-deg plies, F_{ly} is known and therefore F_{cy} is known. F_{cx} equals the resultant horizontal vector; its magnitude is determined by measuring the horizontal distance between fringes near point A in Fig. 5(b). The carrier fringe vectors F_{cx} and F_{cy} are constants throughout the pattern, and their magnitudes are known. For the 0-deg ply near point A, F_{cy}, F_{cx} and the azimuth ϕ_1 of F are drawn. The vector diagram is readily completed, thus establishing the magnitude of F_{ly}, and by eq (6), establishing ϵ_y in the 0-deg ply. Note that the direction of F is verified because it is known from Fig. 5(a) that F_{ly} must be smaller in magnitude in 0-deg plies than in 90-deg plies.

Narrow zones between plies exhibit fringes of azimuth ϕ_2. These represent resin-rich zones that are more compliant in compression than the neighboring plies. The vector procedure is the same. With F_{cx}, F_{cy} and ϕ_2 known, the diagram is completed by drawing the unknown vector F_{ly}. The results are plotted in Fig. 5(d), which shows essentially uniform compressive strains through the thickness of each ply and strong strain peaks in the resin-rich zones between plies. Clearly, this detail cannot be obtained from the load-induced pattern without the use of carrier fringes.

Generalizations and Conclusions

Although the examples given here are specific cases, they illustrate broader categories. The utilization of these techniques for the analysis of fringe gradients can be generalized as follows. (1) To enhance the visibility of a constant or slowly varying fringe gradient, introduce carrier fringes to minimize the gradient in the orthogonal direction. (2) To reveal strong gradients in one direction when the gradients in the orthogonal direction are modest or zero, introduce carrier fringes to increase the modest gradient and use eq (3) to analyze any point. (3) For superior discrimination of gradients in case (2), introduce carrier fringes in both directions to increase the range of fringe slopes present in the pattern and use eq (3) to analyze any point.

Information that can be extracted from moiré patterns can be vastly increased by using carrier fringes. The procedure for extracting the data can be easier and more accurate when carrier fringes are introduced. Fringe vectors provide an effective means of interpreting the patterns. The carrier patterns are easily introduced and controlled by adjustments of the moiré interferometry optical system. Considering its simplicity, the benefits seem magical!

Acknowledgments

The work was sponsored by the National Center for Composite Materials Research, Urbana, Illinois. It was encouraged by Dr. Alan Kushner of The Office of Naval Research. This generous support is gratefully acknowledged.

References

1. Parks, V.J., "Geometric Moiré," Handbook of Experimental Mechanics, ed. A.S. Kobayashi, Chap. 6, Prentice-Hall, Englewood Cliffs, NJ (1987).

2. Chiang, F.-P., "Moiré Method of Strain Analysis," Manual on Experimental Stress Analysis, ed. A.S. Kobayashi, Chap. 6, Soc. for Exp. Mechanics, Bethel, CT (1978).

3. Post, D., "Moiré Interferometry," Handbook of Experimental Mechanics, ed. A.S. Kobayashi, Chap. 7, Prentice-Hall, Englewood Cliffs, NJ (1987).

4. Basehore, M.L. and Post, D., "Displacement Fields (U, W) Obtained Simultaneously by Moiré Interferometry," Appl. Opt., **21** (14), 2558-2562 (July 15, 1982).

5. Czarnek, R., Post, D. and Guo, Y., "Nonuniformities in Composite Panels by Moiré Interferometry," Proc. 1986 SEM Spring Conf. on Exp. Mech., Soc. for Exp. Mech., Bethel, CT (June 1986).

6. Post, D., "Developments in Moiré Interferometry," Opt. Eng., **21** (3), 458-467 (May 1982).

7. Post, D., Dai, F., Guo, Y. and Ifju, P., "Interlaminar Shear Moduli of Cross-ply Laminates: An Experimental Analysis," J. Comp. Mat., **23** (3), 264-279 (March 1989).

8. Post, D., Czarnek, R. and Joh, D., "Shear Strain in a Graphite-PEEK Beam by Moiré Interferometry with Carrier Fringes," EXPERIMENTAL MECHANICS, **27**, 246-249 (Sept. 1987).